Synthesis of HRV signals characterized by predetermined time-frequency structure by means of time-varying ARMA models

Michele Orini [a,b,c,*], Raquel Bailón [a,b], Luca Mainardi [c], Pablo Laguna [a,b]

[a] Communications Technology Group (GTC), Aragón Institute of Engineering Research (I3A), IIS Aragón, University of Zaragoza, 50018 Zaragoza, Spain
[b] CIBER de Bioingeniería, Biomateriales y Nanomedicina (CIBER-BBN), 50018 Zaragoza, Spain
[c] Department of Biomedical Engineering, Politecnico di Milano, 20133 Milan, Italy

ARTICLE INFO

ABSTRACT

In this paper we present two methodologies to generate heart rate variability (HRV) signals characterized by controlled and real-like time-frequency (TF) structure to be used to assess different methods of non-stationary HRV analysis. The synthesized signals are stochastic processes whose TF structure is predetermined by choosing either the time-course of the instantaneous frequencies and powers or the shape of the TF model function. They consist of three steps: (a) choice of the desired TF structure of the signals by choosing a set of design parameters; (b) automatic identification of the parameters of the corresponding models via simple closed-form expressions; (c) synthesis of the desired stochastic signals. Two measures to evaluate the goodness of the simulated signals are also given. Using this framework we were able to model the wide range of non-stationarities observed in heart rate modulation during exercise stress testing and experiments of music-induced emotions. We used the proposed methodology to assess the capability of the smoothed pseudo Wigner–Ville distribution (SPWVD) to quantify HRV patterns. We observed that the SPWVD followed the temporal evolution of the spectral components even when sudden and sharp transitions occur.

© 2011 Elsevier Ltd. All rights reserved.

1. Introduction

The spectral analysis of the heart rate variability (HRV) signal is a non invasive tool widely used to assess the modulation of the autonomous nervous system (ANS) [1]. The spectrum of the HRV signal is characterized by two main spectral components: the low frequency (LF) and high frequency (HF) components, which in human are defined in LF $\in$ [0.04, 0.15 Hz] and HF $\in$ [0.15, 0.40 Hz], respectively. The power in the HF band is considered a measure of parasympathetic activity. The power in the LF band is considered a measure of sympathetic and parasympathetic activity, being its interpretation controversial when, e.g. the respiratory frequency lies in the LF band. Traditional spectral analysis requires stationarity and cannot be applied in a wide range of clinical and physiological studies, such as exercise stress testing, tilt table test, experiments of induced emotions, etc., in which time-frequency (TF) techniques should be preferred. Given that the number of HRV studies which involve TF analysis is increasing [2] and non-stationary signal processing is becoming the rule in cardiovascular analysis, there is a

need of evaluation procedures to assess the performance of TF techniques on each specific application. This can be done by analyzing simulated HRV signals characterized by predetermined real-like time-varying (TV) spectral patterns. In simulation studies, signals related to the autonomic modulation are often modeled as the sum of two deterministic tones embedded in noise [3–6]. Nevertheless, given that the nature of biological signals is not completely deterministic [7], TV autoregressive models are widely used to estimate HRV spectral indices as well as to describe the interactions between cardiovascular signals [2,8–10].

In this study, we propose to use TV autoregressive models to create HRV signals with known and controlled TF structure with the purpose of providing a useful tool for the assessment of different TF methodologies before being used in clinical applications. The proposed framework is then used to evaluate the performance of the smoothed pseudo Wigner–Ville distribution (SPWVD) in non-stationary HRV analysis. Our attention is focused on exercise stress testing and experiments of music-induced emotions. Exercise stress testing [6,8] is a common test during which cardiovascular parameters vary quickly within a wide range of values. Recently, indices of HRV during this test have been used in the diagnosis of coronary artery diseases [11–13]. The validation of TF techniques used in the HRV analysis during experiments of music-induced emotions deserves attention since in the recent years the interest in therapeutic applications of music has increased, as well

* Corresponding author at: Communications Technology Group (GTC), Aragón Institute of Engineering Research (I3A), IIS Aragón, University of Zaragoza, 50018 Zaragoza, Spain.
E-mail addresses: michele@unizar.es, michele.orini@mail.polimi.it (M. Orini).

as the effort to understand the relationship between music features and physiological patterns [14,15].

The paper is organized as follows: two frameworks for the simulation of non-stationary stochastic signals are presented in Section 2. The modeling of HRV signals during exercise stress testing and experiments of music-induced emotions is considered in Section 3. The SPWVD is described in Section 4. Results and discussion are presented in Sections 5 and 6, respectively.

2. Synthesis of non-stationary random processes

2.1. General framework

A time-varying autoregressive moving average (TV-ARMA) model can be used to describe non stationary signals:

$$x(n) = -\sum_{k=1}^{\tilde{p}} a_k(n)x(n-k) + \sum_{k=0}^{\tilde{q}} b_k(n)\xi(n-k) \tag{1}$$

where $a_k(n)$ and $b_k(n)$ are TV coefficients, $\tilde{p}$ and $\tilde{q}$ are the orders of the AR and MA part of the model, and $\xi(n)$ is a zero-mean unit-variance white noise. The TV transfer function of (1), $H(n, z)$, and the TF model function of the random process $x(n)$, $S(n, f)$, can be derived from the coefficients of the model as:

$$H(n, z) = \frac{\sum_{k=0}^{\tilde{q}} b_k(n)z^{-k}}{1 + \sum_{k=1}^{\tilde{p}} a_k(n)z^{-k}} = \frac{\prod_{k=1}^{\tilde{q}}(z - z_k(n))}{\prod_{k=1}^{\tilde{p}}(z - p_k(n))} b_0(n)z^{(\tilde{p}-\tilde{q})} \tag{2}$$

$$S(n, f) = \left| H(n, f) \right|^2 = \left[\frac{b_0^2(n)\prod_{k=1}^{\tilde{q}}\left|z - z_k(n)\right|^2}{\prod_{k=1}^{\tilde{p}}\left|z - p_k(n)\right|^2} \right]_{z=e^{j2\pi f}} \tag{3}$$

where $f \in [-0.5, \ 0.5]$, while $z_k(n) = |z_k(n)|e^{j\angle z_k(n)}$ and $p_k(n) = |p_k(n)|e^{j\angle p_k(n)}$ are the zeros and poles of $H(n, z)$. Poles and zeros are numbered according to their phase, as $0, \ldots, \angle p_1(n)$, $\angle p_2(n), \ldots, 2\pi$. When a complex pole is sufficiently close to the unit circle and far from other poles, its power is given by the pole residue [16,17]:

$$P_i(n) = \mathcal{R}\left[\frac{\prod_{k=1}^{\tilde{q}}(p_i(n) - z_k(n))\prod_{k=1}^{\tilde{q}}(p_i^{-1}(n) - z_k^*(n))b_0^2(n)}{p_i(n)(p_i^{-1}(n) - p_i^*(n))\prod_{\substack{k=1 \\ k \neq i}}^{\tilde{q}}(p_i - p_k(n))(p_i^{-1}(n) - p_k^*(n))} \right] \tag{4}$$

Given a predetermined $S(n, f)$, we look for simple closed-form expressions which allow to estimate the polar configuration of the corresponding transfer function $H(n, z)$. The rational for searching these closed-form expressions is to easily design any suitable spectral pattern for the stochastic processes being used in simulation studies. The simulation process involves three steps: (a) choice of the desired TF structure of $x(n)$, which is defined by a set of design parameters; (b) estimation of the corresponding $H(n, z)$ and (c) synthesis of the desired signals, by regressing the model coefficients with $\xi(n)$ as in (1). Two general frameworks, which differ in the choice of the parameters which characterize the TF structure of the signals, are proposed. The first framework (I-FS) is proposed to reproduce signals characterized by a desired TF model function $S(n, f)$, while the second one (II-FP) is proposed to generate signals characterized by predetermined instantaneous frequencies and powers. Since in TF analysis the HRV signal usually presents at least two well

defined spectral peaks, corresponding to the LF and HF components, we only considered those zero-pole configurations yielding $S(n, f)$ with two well resolved narrow-band spectral peaks.

2.2. Framework I-FS

In framework I-FS, TV-ARMA models are used to reproduce a predetermined TF model function $S(n, f)$ composed by spectral peaks of instantaneous amplitude $S(n, f_i(n))$ and normalized frequency $f_i(n)$, with $i \in [1 : \tilde{p}]$. The desired shape of $S(n, f)$ is approximated by $f_i(n)$, $S(n, f_i(n))$ and by appropriately positioning the zeros $z_k(n)$ in the polar plane (see Section 2.4 for details). To estimate $H(n, z)$, (3) should be solved with respect to $p_k(n)$. This is done by considering that the amplitude of a spectral peak centered on $f_i(n)$ is:

$$S(n, f_i(n)) = \left[\frac{\prod_{k=1}^{\tilde{q}}\left|z - z_k(n)\right|^2}{\prod_{k=1}^{\tilde{p}}\left|z - p_k(n)\right|^2} b_0^2(n) \right]_{z=e^{j2\pi f_i(n)}} \tag{5}$$

where $\left|z - p_k(n)\right|$ represents the distance between the point $z = e^{j2\pi f_i(n)}$, located on the unit circle at phase $2\pi f_i(n)$, and the pole $p_k(n)$. Every pole is assumed to correspond to a spectral peak. Given that $z_k(n)$ are design parameters, the numerator of (5) is a known quantity $N_i(n)$, while the terms in the denominator are estimated by means of the cosine formula:

$$|e^{j2\pi f_i(n)} - p_k(n)|^2 = |p_k(n)|^2 + A_{i,k}(n)|p_k(n)| + 1 \tag{6}$$

$$A_{i,k}(n) = -2\cos(2\pi f_i(n) - \angle p_k(n)); \quad i, k \in [1, \tilde{p}] \tag{7}$$

Inserting (6) in (5) we obtain a set of equations $\mathbb{E}_i$:

$$\mathbb{E}_i: \prod_{k=1}^{\tilde{p}}(|p_k(n)|^2 + A_{i,k}(n)|p_k(n)| + 1) = \frac{N_i(n)}{S(n, f_i(n))}b_0^2(n) \tag{8}$$

with $i \in [1, \tilde{p}]$. The solution of (8) provides the $|p_k(n)|$ and $b_0(n)$ which define the pole configuration of $H(n, z)$ and consequently the coefficients $a_k(n)$ and $b_k(n)$. To model the HRV signal, which in short-term analysis is characterized by the simultaneous presence of two main spectral components, four poles are used ($\tilde{p} = 4$). In Fig. 1, the graphic representation of (5) for a model of order $(\tilde{p}, \tilde{q}) = (4, 2)$ evaluated at $f_i(n_0) = f_{\text{LF}}(n_0)$ is shown. Black and gray arrows represent the factors which appear in the denominator and in the numerator of (5), respectively. The model includes two complex conjugate poles associated to the LF component, namely $p_{\text{LF}}(n) = p_1(n) = p_4^*(n)$, and two complex conjugate poles associated to the HF component, namely $p_{\text{HF}}(n) = p_2(n) = p_3^*(n)$. In this example $z_1(n)$ and $z_2(n)$ are placed on the unit circle and constrain the spectrum to vanish at frequency $\pm(1/2\pi)\angle z_1(n)$. The design parameters are: $f_{\text{LF}}(n)$, $f_{\text{HF}}(n)$, $S(n, f_{\text{LF}}(n))$, $S(n, f_{\text{HF}}(n))$ and $z_k(n)$, while the unknown quantities are $|p_k(n)|$ and $b_0(n)$. After rearrangement, system (8) can be written:

$$\begin{cases} \dfrac{\prod_{k=1}^{4}(|p_k(n)|^2 + A_{\text{LF,k}}(n)|p_k(n)| + 1)}{\prod_{k=1}^{4}(|p_k(n)|^2 + A_{\text{HF,k}}(n)p_k(n)| + 1)} = \dfrac{N_{\text{LF}}(n)S(n, f_{\text{HF}}(n))}{N_{\text{HF}}(n)S(n, f_{\text{LF}}(n))} \\[4mm] b_0^2(n) = \dfrac{S(n, f_{\text{HF}}(n))}{N_{\text{HF}}(n)}\prod_{k=1}^{4}(|p_k(n)|^2 + A_{\text{HF,k}}(n)|p_k(n)| + 1) \end{cases} \tag{9}$$

A restriction should be introduced to match the number of equations with the number of unknowns. To this end, the magnitude
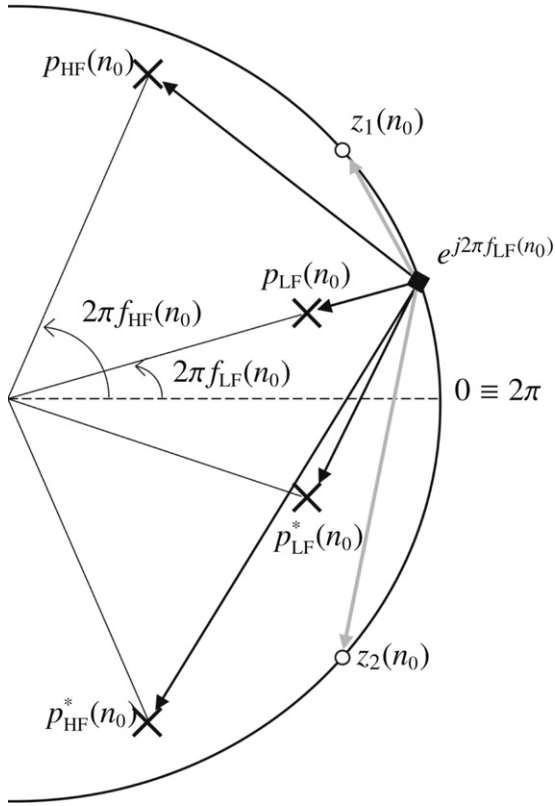
Fig. 1. Configuration of a TV-ARMA of order (4,2) for $n = n_0$. Crosses and circles represent poles and zeros, respectively, while black and gray arrows correspond to the term in the denominator and numerator of (5), respectively.

of two complex conjugate poles is fixed to a constant value. As shown in the following, this restriction gives the possibility to further increase the control of $S(n, f)$. Fixing the magnitude of the LF poles to a constant value $|p_1(n)| = |p_4(n)| = |p_{LF}|$ the first equation of system (9) takes the closed-form of a quartic equation:

$$|p_{HF}(n)|^4 + C_1(n)|p_{HF}(n)|^3 + C_2(n)|p_{HF}(n)|^2 + C_1(n)|p_{HF}(n)| + 1 = 0$$
(10)

where

$$C_1(n) = \frac{(A_{LF,2}(n) + A_{LF,3}(n)) - \alpha(n)(A_{HF,2}(n) + A_{HF,3}(n))}{1 - \alpha(n)}$$
(11)

$$C_2(n) = \frac{(2 + A_{LF,2}(n)A_{LF,3}(n)) - \alpha(n)(2 + A_{HF,2}(n)A_{HF,3}(n))}{1 - \alpha(n)}$$
(12)

$$\alpha(n) = \frac{S(n, f_{HF}(n))N_{LF}(n) \displaystyle\prod_{k=\{1,4\}} (|p_{LF}|^2 + A_{HF,k}(n)|p_{LF}| + 1)}{S(n, f_{LF}(n))N_{HF}(n) \displaystyle\prod_{k=\{1,4\}} (|p_{LF}|^2 + A_{LF,k}(n)|p_{LF}| + 1)}$$
(13)

Eq. (10) has a real solution whenever:

$$\left[\frac{1}{2}\left(-C_1 + \sqrt{C_1^2 - 4(C_2 - 2)}\right)\right]^2 - 4 < 0$$
(14)

Once that the magnitude of the HF poles, $|p_{HF}(n)|$, has been estimated, the parameter $b_0(n)$ is obtained by replacing $|p_{HF}(n)|$ in the second equation of (9). In the case in which the magnitude of the HF poles $|p_2(n)| = |p_3(n)| = |p_{HF}|$ was used as design parameter, $|p_1(n)| = |p_4(n)|$ would be obtained using (10)–(13) and replacing $A_{i,2}$ with $A_{i,1}$, and $A_{i,3}$ with $A_{i,4}$, with $i \in \{LF, HF\}$, respectively.

2.3. Framework II-FP

In this case, the TF structure of the signals is predetermined by fixing instantaneous frequencies $f_i(n)$ and powers $P_i(n)$, rather than $f_i(n)$ and $S(n, f_i(n))$, as in I-FS. The pole-zero configuration associated to $f_i(n)$ and $P_i(n)$ can be estimated by using (4). At every n, the power associated to the pole $p_i(n)$ depends on the whole pole-zero configuration, i.e. on the whole set of complex numbers $p_i(n) - p_k(n)$, $p_i^{-1}(n) - p_k^*(n)$, $p_i(n) - z_k(n)$ and $p_i^{-1}(n) - z_k^*(n)$. The explicit form of (4) is highly non-linear in $|p_i(n)| e^{j\angle p_i(n)}$. Nevertheless, as shown in [16], by using an autoregressive model (i.e. not considering $z_k(n)$) and placing the poles very close to the unit circle $(1 - |p_i(n)| \ll 1)$, one can approximate $p_i^{-1}(n)$ with $p_i^*(n)$ and rewrite (4) as:

$$P_i(n) \approx \frac{b_0^2(n)}{\left(|P_i(n)| - \frac{1}{|P_i(n)|}\right)\displaystyle\prod_{\substack{k=1 \\ k \neq i}}^{\tilde{p}} |P_i(n) - P_k(n)|^2}; \quad i = \{1, \tilde{p}\};$$
(15)

When $i = \{LF, HF\}$, (15) represents a system of 2 equations in $|p_{LF}(n)|$, $|p_{HF}(n)|$ and $|b_0(n)|$. Similar to what previously done in (8)–(10), the solution is found by: (i) use the magnitude of two complex-conjugate poles as a design parameters, (ii) rewrite (15) in the form $P_{LF}(n)/P_{HF}(n) = [\ldots]$ and (iii) estimate from this new expression the magnitude of the other 2 complex-conjugate poles; (iv) estimate $b_0(n)$ by solving one of the equations of system (15). It can be shown that using $|p_1(n)| = |p_4(n)| = |p_{LF}|$ as design parameter, one can easily estimate the corresponding $|p_{HF}(n)|$ by solving

$$|p_{HF}(n)|^3 - |p_{HF}(n)| + C(n) = 0$$
(16)

where

$$C(n) = \frac{P_{LF}(n)}{P_{HF}(n)}\left(\frac{\sin(2\pi f_{LF}(n))}{\sin(2\pi f_{HF}(n))}\right)^2 (|p_{LF}| - |p_{LF}|^3)$$
(17)

In the case in which $|p_2(n)| = |p_3(n)| = |p_{HF}|$ was used as design parameter, $|p_1(n)| = |p_4(n)| = |p_{LF}(n)|$ would be obtained using (16) and (17) and replacing subscript LF with HF and subscript HF with LF. The incomplete cubic equation (16) has an acceptable real solution for those n for which $C(n) \in (-2/\sqrt{27}, 2/\sqrt{27})$.

2.4. Design parameters

Design parameters necessary to define the desired TF structure of the signals are $f_i(n)$, $S(n, f_i(n))$, with $i = \{LF, HF\}$, and $z_k(n)$, in the case of I-FS and $f_i(n)$, $P_i(n)$ in the case of II-FP. In both cases, the magnitude of one of the two complex-conjugate poles is fixed and the other one is estimated. The positioning of the poles used as design parameters can be used to improve the control of the shape of the model function $S(n, f)$: by moving the poles closer to the unit circle the spectral peaks get sharper and their bandwidth is reduced.

In the case of framework I-FS, zeros are used to predetermine desirable spectral features. As shown in Fig. 2, they can be used to control the degree of overlapping of the spectral peaks. Model functions shown in the upper, middle and lower panels share the same $f_i(n_0)$, $S(n_0, f_i(n_0))$ as well as the magnitude of the poles used as design parameters. Those on the left are obtained by means of AR models, while those on the right by means of an ARMA model of order (4,10). In these graphics, circles represent the phase of zeros $z_k(n_0)$, with $k = \{1, 2, 3\}$. It is shown that without changing the magnitude of the pole used as design parameter, and by moving $z_k(n)$ closer to the unit circle, $S(n_0, f)$ takes lower values at frequency $(1/2\pi)\angle z_k(n)$ and the spectral peaks are better resolved.

2.5. Evaluation of the models for non-stationary HRV signals

Due to the stochastic nature of the signals and to the limited number of realizations of the model, the TF distribution of the stochastic process, obtained by averaging among realizations, always presents a fluctuation around $S(n, f)$. This fluctuation represents a sort of intrinsic uncertainty of the simulated signals and is quantified by means of two measures. The first one is a spectral distance, defined as the normalized L1-norm of the difference between $S(n, f)$ and the estimated TF distribution of the stochastic process $\bar{W}_x(n, f)$:

$$d_W = \frac{\|\bar{W}_x(n,f) - S(n,f)\|_{l_1}}{\|S(n,f)\|_{l_1}} \tag{18}$$

$$\bar{W}_x(n,f) = \frac{1}{R}\sum_{r=1}^{R} W_x(n,f;r) \tag{19}$$

where $W_x(n, f;r)$ is the Wigner–Ville distribution of one realization $x(n;r)$ [18,19]. Distance d_W is specially sensitive to the correct TF localization of the spectral components. The second measure is obtained by comparing the total power $P_{TOT}(n)$, obtained by integrating $S(n, f)$ with respect to f, with the instantaneous powers of the simulated signals:

$$e(n) = \frac{\frac{1}{R}\sum_{r=1}^{R} x^2(n;r) - P_{TOT}(n)}{P_{TOT}(n)} \tag{20}$$

The temporal mean and standard deviation of $e(n)$, denoted as μ_e and σ_e, is used to assess the capability of the model to generate signals characterized by the desired instantaneous power. For a given number of realizations R, measures d_W and $e(n)$ depend on the pole-zero configuration given by $p_k(n)$, $z_k(n)$, $b_0(n)$ and will be used in the following to assess the effect of the design parameters as well as to compare the frameworks.

3. Applications

In this section, the dynamics observed in the HRV signal during exercise stress testing (EST) and experiments of music-induced emotions (MIE) are modeled. In both situations, the evaluation of frameworks I-FS and II-FP is done as follows: (i) framework I-FS is used: signals are modeled by fixing $f_i(n)$, $S(n, f_i(n))$ and by choosing $z_k(n)$ and $|p_{LF}|$ as to obtain the desired model function $S(n, f)$, which will be used in the evaluation; (ii) the instantaneous power of LF and HF components, $P_{LF}(n)$ and $P_{HF}(n)$, are estimated from this model function, and (iii) they are used as design parameters of framework II-FP, whose model function will be estimated and used to assess the uncertainty of the simulated signals obtained with framework II-FP.

The TF structure of the simulated signals is shown in Fig. 3(a) and (b), where $F_i(n) = f_i(n)F_s$, being F_s the sampling rate. In both cases, signals are characterized by epochs of mild and abrupt variations (indicated as T_1 and T_2, respectively), which correspond to different degrees of non-stationarity. The degree of non-stationarity, reported in Table 1, is quantified by:

$$\bar{F}'_i = \frac{F_s}{N_T} \sum_{n=n_b}^{n_b+N_T-1} |F_i(n) - F_i(n-1)|, \quad [\text{Hz}\,\text{s}^{-1}] \tag{21}$$

$$\bar{S}'_i = \frac{F_s}{N_T} \sum_{n=n_b}^{n_b+N_T-1} \frac{|S(n, f_i(n)) - S(n, f_i(n-1))|}{S(n_0, f_i(n_0))}, \quad [\%\,\text{s}^{-1}] \tag{22}$$

Table 1
Simulation setup.

Parameters of I-FS framework	EST		MIE	
	T_1	T_2	T_1	T_2
Length [s]	360	150	38	42
$\bar{F}'_{LF}$ [mHz s^{-1}]	0	0	0.9	1.6
$\bar{F}'_{HF}$ [mHz s^{-1}]	1.1	2.2	0.3	3.2
$\bar{S}'_{LF}$ [% s^{-1}]	0.14	0.28	1.14	2.3
$\bar{S}'_{HF}$ [% s^{-1}]	0.25	0.28	0.8	1.4
Order	(4,8)		(4,10)	
F_s [Hz]	2		2	
R	1000		1000	
$|p_{LF}|$	0.905		0.870	

where N_T is the number of time samples of intervals T_1 or T_2, n_b is the first time sample of each interval, $i \in \{LF, HF\}$ and $n_0 = 1$.

3.1. Exercise stress testing (EST)

As shown in Fig. 3(a), in this simulation the HRV spectral components are assumed to vary linearly [6]. F_{LF} is constant over time, while $F_{HF}(n)$ increases and decreases during effort (T_1) and recovery (T_2), respectively. Changes in $S(n, f_{HF}(n))$ simulates the withdrawal of the parasympathetic modulation (-70% in the first 3 min) and the restoration of baseline values during recovery ($+50\%$ in 3 min). From 3 min after the onset of the exercise until the peak stress $S(n, f_{HF}(n))$ slightly increases, simulating the effect of the stretch of the sinus node [20]. A model of order (4,8) with $|p_{LF}| = 0.905$ is used. Details about the choice of this specific value are given in the following. Zeros are placed on the unit circle and have TV phase. Zero $z_1(n)$, fixed at DC, cancels the contribution around $f = 0$ Hz, which in TF analysis is usually filtered out; $z_2(n) = z_8^*(n)$, with phase $\pi(f_{LF}(n) + f_{HF}(n))$, lies in between LF and HF poles, to separate the spectral peaks, which otherwise would overlap; $z_3(n) = z_7^*(n)$, with phase $\pi(3f_{HF}(n) - f_{LF}(n))$, is symmetric to $z_2(n)$ with respect to $f_{HF}(n)$ and makes the HF peak symmetric; zero $z_4(n) = z_6^*(n)$, with phase $\frac{\pi}{2}(3f_{HF}(n) - f_{LF}(n) + 1)$ and $z_5(n) = \pi$, cancel undesired contributions introduced by the other ones in $f > f_{HF}(n)$.

3.2. Experiments of music-induced emotions (MIE)

Parameters $F_i(n)$ and $S(n, f_i(n))$ were derived from the time-course of the LF and HF components of an original HRV signal recorded during an experiment of music-induced emotions [15]. In that experiment, participants listened to different kind of musical stimuli, each one of a duration of about 90 s, and characterized by different emotional valence. The pattern of response of the HRV signal, shown in Fig. 3(b), is characterized by two phases: an early fast epoch in which abrupt changes occur (T_2), and a later epoch of adaptation in which spectral parameters changed gradually (T_1). The time-course of spectral indices of Fig. 3(b) is derived by low-pass filtering the time-course of the parameters obtained by TF analysis of the HRV of a subject listening to an excerpt of pleasant music [15]. As also reported in Table 1, changes in T_2 are particularly abrupt: $S(n, f_{LF}(n))$ and $S(n, f_{HF}(n))$ decreases by about 70% and 40% in the first 13 s. In this application, a model of order (4,10), with $|p_{LF}| = 0.870$, is used. Zeros are placed on the unit circle and have TV phase. Zeros $z_1(n)$, $z_2(n) = z_{10}^*(n)$ and $z_3(n) = z_9^*(n)$ are located as in simulation EST, while, in order to cancel contributions in $f > f_{HF}(n)$, $z_4(n) = z_8^*(n)$, $z_5(n) = z_7^*(n)$ and $z_6(n)$ are evenly distributed between $z_3(n)$ and π, i.e. with phases equal to $\frac{\pi}{3}(6f_{HF}(n) - 2f_{LF}(n) + 1)$, $\frac{\pi}{3}(3f_{HF}(n) - f_{LF}(n) + 2)$ and π, respectively.
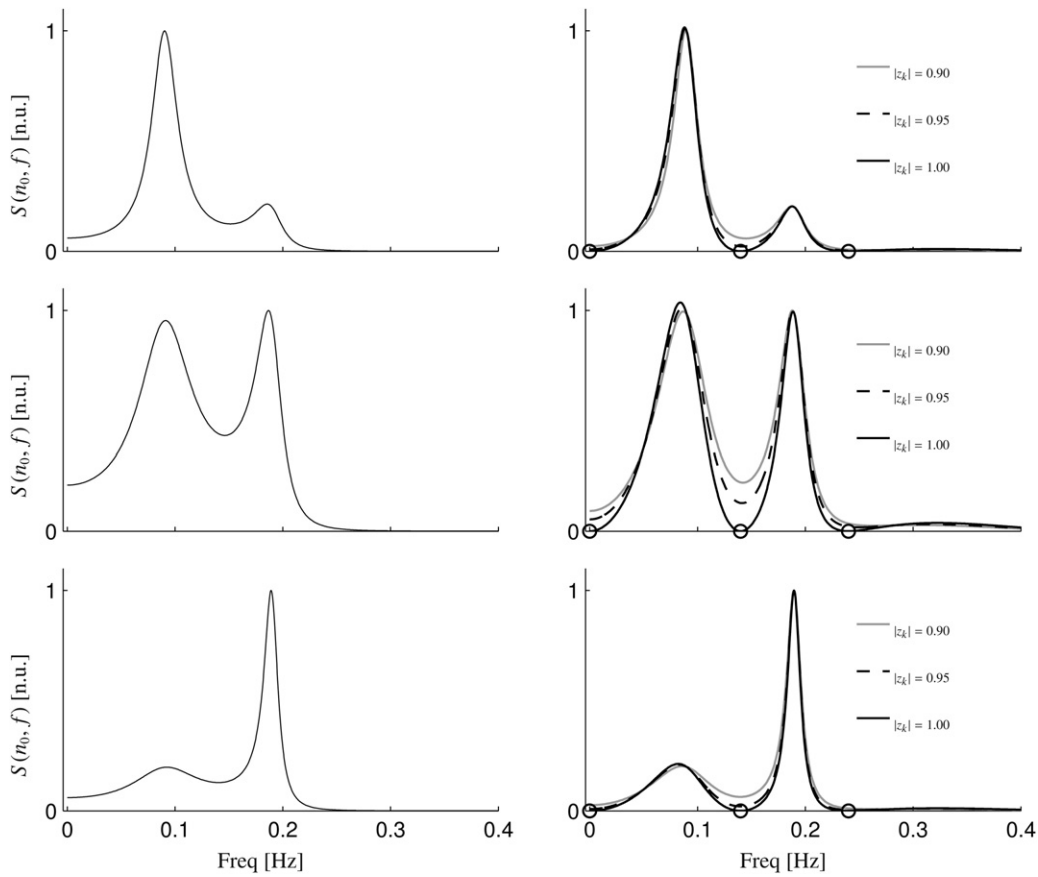
Fig. 2. Influence of $z_k(n)$ on the model function. $S(n_0, f)$ are modeled by means of AR models (left) and ARMA models of order (4,10) (right). Circles represent the phase of $z_k(n_0)$, with $k = \{1, 2, 3\}$. All $z_k(n_0)$ have the magnitude reported in the legend. Zeros $z_k(n_0)$, with $k > 3$, are associated to a frequency $f > 0.4$ Hz and are not shown.

4. Evaluation of the SPWVD

The framework presented in the previous sections is used to evaluate the performance of the SPWVD [18] in non-stationary HRV analysis. Among the different TF and TV methods which have been applied to the study of the cardiovascular variability [2], the SPWVD is one of the most interesting, since it provides an independent control of the time and frequency resolution. It is defined as the
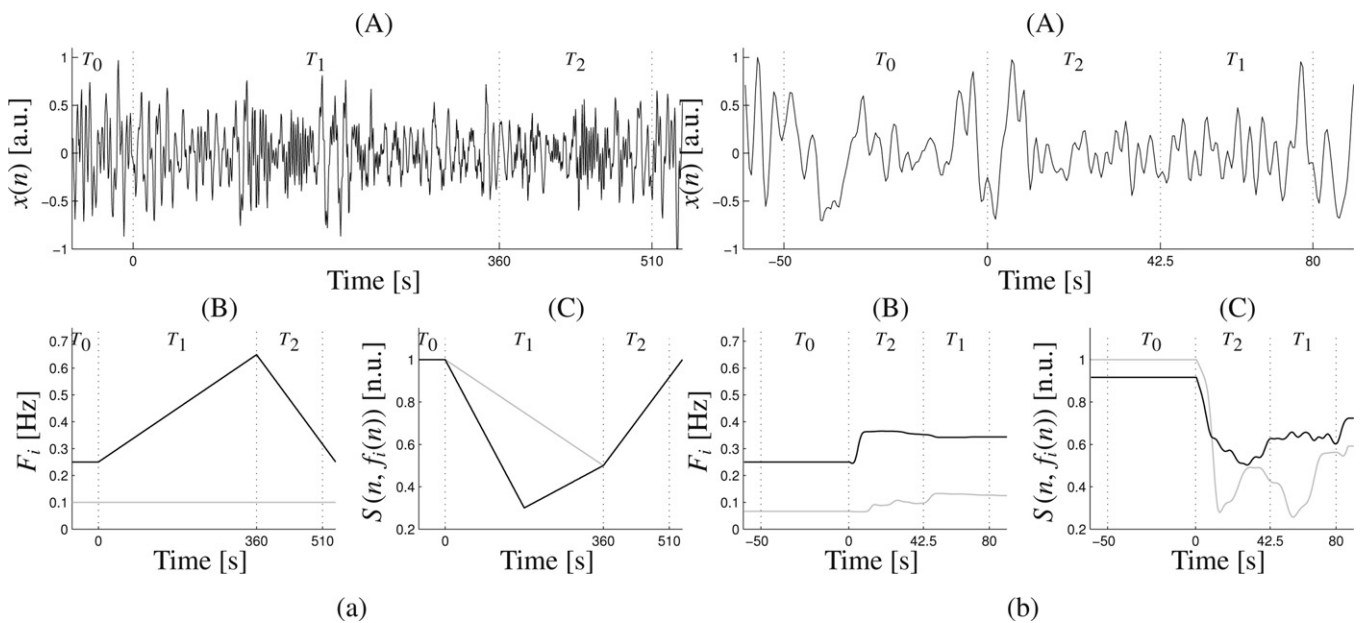

Fig. 3. Modeling HRV during: (a) exercise stress testing (EST) and (b) experiment of music-induced emotions (MIE). (A) A simulated HRV signal $x(n)$; (B) instantaneous frequency and (C) spectral amplitude of the LF (in gray) and HF (in black) components. T_0, T_1 and T_2 represent epochs of stationarity, slow and fast variations. Note that temporal axes are different.
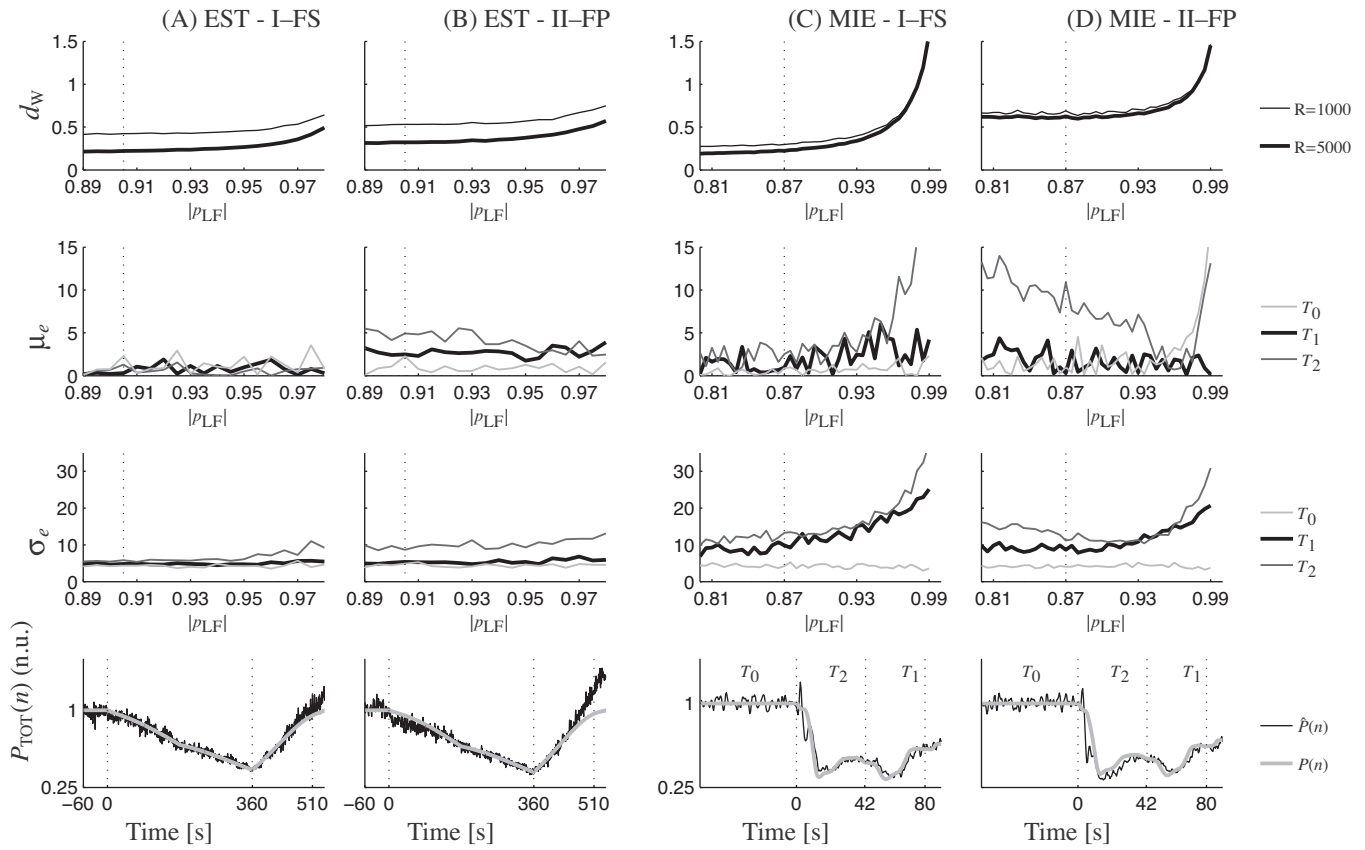
Fig. 4. Model evaluation: (A and B) exercise stress testing; (C and D) experiment of music-induced emotions; (A and C) I-FS framework; (B and D) II-FS framework. The intrinsic uncertainty of the simulated signals is evaluated by means of the spectral distance d_W (top graphic) and the mean and the standard deviation of $e(n)$ (second and third lines of graphics). Vertical dotted lines marked the $|p_{LF}|$ used to generate the signals for the evaluation of the SPWVD. Lower graphics: $P_{TOT}(n)$ estimated from $S(n,f)$ and power estimated form the signals with $R = 1000$. See Section 2.5 for details.

Fourier transform of the generalized autocorrelation function of $x_a(n)$, the complex analytic signal representation of the original real signal $x(n)$ [18]:

$$\hat{S}(n,f) = \hat{S}(n,\nu)|_{\nu=2f}, \quad f \in [-0.25, 0.25] \tag{23}$$

$$\hat{S}(n,\nu) = 2 \sum_{k=-K+1}^{K-1} \left[|h(k)|^2 \sum_{n'=-N+1}^{N-1} \left[g(n') x_a(n+n'-k) x_a^*(n+n'+k) \right] \right]$$
$$\times e^{-j2\pi k\nu}, \quad \nu \in [-0.5, 0.5] \tag{24}$$

In (23), a variable change is used since the SPWVD in (24) has the spectral peaks at twice the frequency of the spectral components of $x_a(n)$. Functions $g(n')$ and $|h(k)|^2$ are the time and frequency smoothing kernels used to reduce the interference terms, while n and f are the discrete time index and the normalized frequency, respectively. In this study, the rectangular window $g(n) = \frac{1}{2N-1}$, with $n = (-N+1), \ldots, (N-1)$, and the exponential function $|h(k)|^2 = e^{-\gamma|k|}$ were used. The degree of time and frequency smoothing depends on the length of the rectangular window $(2N-1)$ and on the damping factor of the exponential window γ. To estimate the time-course of the HRV spectral indices the traditional LF band, $B_{LF} = [0.04, 0.15]$ Hz and a TV respiration-dependent HF band, $B_{HF}(n) = F_r(n) + [-0.125, 0.125]$ Hz, are used [21]. Here, the respiratory rate $F_r(n)$ is assumed to be equal to $F_{HF}(n)$. In real data analysis a direct or ECG-derived estimation of respiratory rate could be used to dynamically adjust the HF band. Instantaneous frequencies from the model ($F_{LF}(n)$, $F_{HF}(n)$) and from TF analysis ($\hat{F}_{LF}(n)$, $\hat{F}_{HF}(n)$) are obtained as the peak frequency of $S(n,f)$ from (3) and of $\hat{S}(n,f)$ from (23) in B_{LF}, $B_{HF}(n)$, respectively. In both frame-

works, instantaneous powers, $P_{LF}(n)$, $P_{HF}(n)$, $P_{TOT}(n)$ and $\hat{P}_{LF}(n)$, $\hat{P}_{HF}(n)$, $\hat{P}_{TOT}(n)$ are obtained by integrating $S(n,f)$ and $\hat{S}(n,f)$ on B_{LF}, $B_{HF}(n)$ and on the entire spectrum, respectively. The estimation error between the time-course of a general HRV index $\phi(n)$ and its estimate $\hat{\phi}(n)$ is calculated as:

$$E_\phi(n) = \frac{\frac{1}{R}\left(\sum_{r=1}^{R} \hat{\phi}_r(n)\right) - \phi(n)}{\phi(n)} \tag{25}$$

where $\phi(n) \in \left\{ F_{LF}(n), F_{HF}(n), P_{LF}(n), P_{HF}(n), P_{TOT}(n) \right\}$ and R is the number of realizations of the model.

5. Results

5.1. Evaluation of the models for non stationary HRV signal

In Fig. 4, the intrinsic uncertainty of signals obtained by means of frameworks I-FS and II-FP is shown for both simulations EST and MIE. The uncertainty was assessed by measures d_W and $e(n)$, estimated from (18) to (20), where, for each framework, the corresponding model function $S(n,f)$ was used. As shown in Fig. 4, the intrinsic uncertainty of the simulated signals always decreased with $|p_{LF}|$, i.e. the magnitude of the pole used as design parameter. This indicates that signals characterized by wide spectral peaks are generated more reliably than signals characterized by narrow spectral peaks. As a rule of thumb, to minimize the intrinsic uncertainty of the signals, one should give to the poles used as design parameters the lowest magnitude which at the same time allows
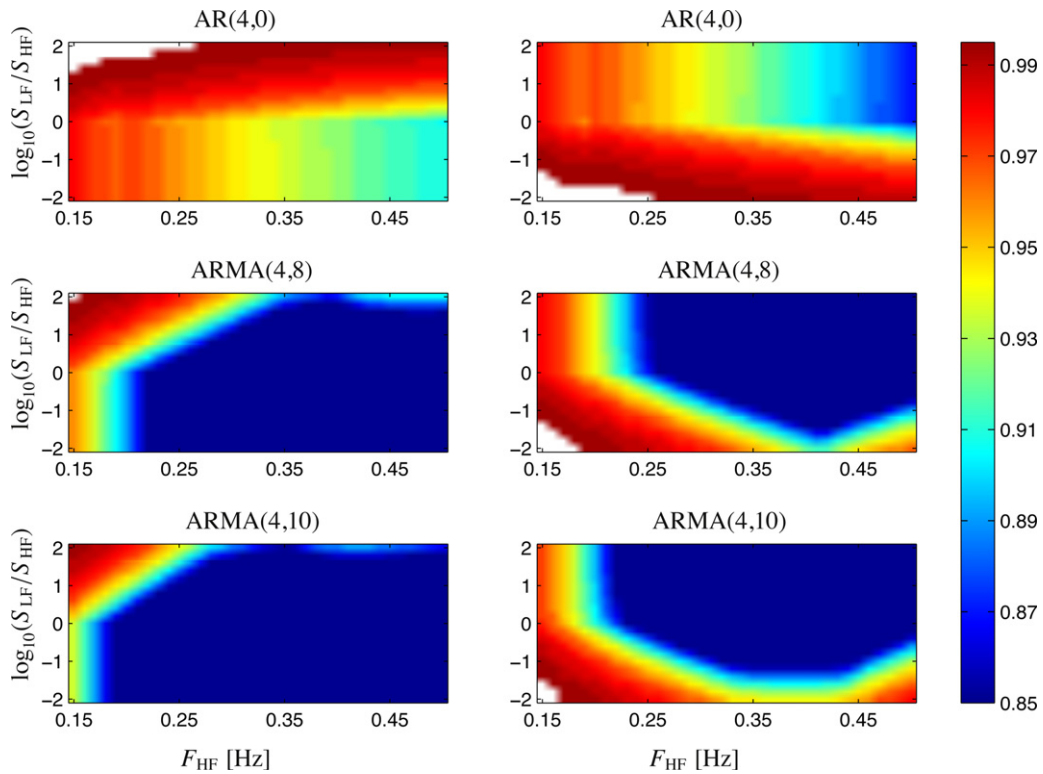
Fig. 5. Robustness and contribution of z_k for the I-FS framework. Left panels: $|p_{LF}|$ is used as design parameters; right panels: $|p_{HF}|$ is used as design parameters; upper, middle and lower graphics refer to models of order (4,0), (4,8) and (4,10). The lowest $|p_{LF}|$ (on the left) and the lowest $|p_{HF}|$ (on the right) which allowed to reproduce real-like HRV signals are color coded. White color means that no suitable solution is available. In y-label S_{LF} stand for $S(f_{LF})$. (For interpretation of the references to color in this figure legend, the reader is referred to the web version of the article.)

the generation of a model function which complies with the specifications. This heuristic method was used to select the values of $|p_{LF}|$ used in simulation EST and MIE. Comparison of results reported in column (A)–(B) and (C)–(D) of Fig. 4 shows that the spectral distance d_W as well as the mean and the standard deviation of $e(n)$ were lower for signals obtained by using framework I-FS than II-FP. As shown in Fig. 4, by increasing the number of realizations of the model, R, the intrinsic uncertainty decreased. The comparison between $P_{TOT}(n)$ and the power estimated directly from the signal as in (20) is reported in the lower graphic of Fig. 4 and shows that the simulated signals followed on average the desired dynamics, even in epoch T_2 of simulation MIE, during which the instantaneous power dramatically decreased while $F_{HF}(n)$ increased almost stepwise.

To assess whether the presented methodology can reproduce a much wider range of spectral configurations than those considered here, and to assess how the use of zeros affects the intrinsic uncertainty of the models, simulations EST and MIE were modified and different configurations were tested. In the following, index n is omitted. Spectral parameters were chosen as: $F_{LF} = 0.09$ Hz, $F_{HF} = \{0.15, 0.16, \ldots, 0.5\}$ Hz and $\log_{10}\left(S(f_{LF})/S(f_{HF})\right) = \{-2, -1.8, \ldots, 2\}$. The magnitude of one couple of complex-conjugate poles was fixed at $\{0.850, 0.855, \ldots, 0.995\}$ and the magnitude of the other poles was estimated by using the closed-form expressions of framework I-FS (10). Models with the following configurations were tested: AR model, ARMA (4,8) as in simulation EST, and ARMA (4,10) as in simulation MIE. To accept $|p_{HF}|$ (or $|p_{LF}|$) as a possible solution, the corresponding model function should verify the following conditions: (i) very low frequency (VLF) is low $S(0) \leq 0.15 \min[S(f_{LF}), S(f_{HF})]$; (ii) LF and HF spectral peaks are well resolved: $S((f_{LF} + f_{HF})/2) \leq 0.25 \min[S(f_{LF}), S(f_{HF})]$; (iii) components with central frequency higher than HF are low $S(f > f_{HF}) \leq 0.15 \min[S(f_{LF}), S(f_{HF})]$. Fig. 4 shows that, when-

ever possible, solutions characterized by a polar configuration with poles of low magnitude should be preferred to configurations with poles of high magnitude, since the lower the magnitude of the poles, the better the simulated signals will reproduce the desired spectral patterns. Results reported in Fig. 5 give, for the whole set of configurations, the lowest magnitude of the poles used as design parameter for which a suitable solution existed. Results reported on the left (right) correspond to the case in which $|p_{LF}|$ ($|p_{HF}|$) was used as design parameter and $|p_{HF}|$ ($|p_{LF}|$) was estimated. In the white regions no suitable solution was found, either because (10) had no solution or because $S(n, f)$ did not comply with the specifications. Fig. 5 shows that: (i) framework I-FS is robust: the only few cases in which a suitable solution was not found corresponded to extreme configurations for which the HRV signal may be better modeled as monocomponent; (ii) for a same configuration, ARMA models allowed to use poles with lower magnitude than AR models, which in turn allows one to generate signals characterized by lower uncertainty; (iii) solutions for low F_{HF} are possible only with poles of high magnitude; (iv) to model HRV signals in which $S(f_{LF}) \gg S(f_{HF})$, it is preferable to use as design parameter $|p_{HF}|$ and estimate $|p_{LF}|$, since, as shown in the right-side panels, in this way it is possible to find appropriate polar configurations by using poles with lower magnitude than if $|p_{LF}|$ was used as design parameter and $|p_{HF}|$ was estimated (as in the left-side panels).

5.2. Evaluation of SPWVD

For both simulations EST and MIE, 1000 signals were generated with a sampling frequency of 2 Hz. In the calculation of the SPWVD we used 9 different kernels. The width of $g(n)$ gave a time resolution of about $\{20, 35, 50\}$ and $\{5, 15, 25\}$ seconds for simulation EST and MIE, respectively, while in both simulations $|h(k)|^2$ gave a frequency resolution of $\{0, 7, 13\}$ mHz. Time and frequency resolu-
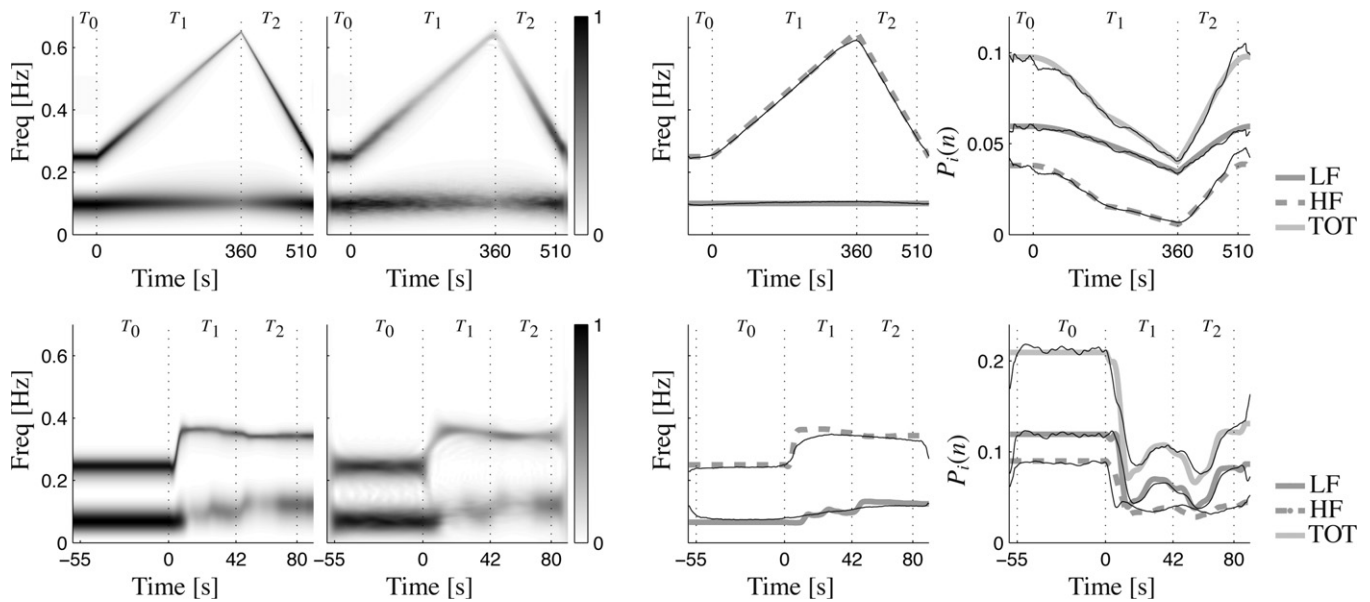
Fig. 6. Model and estimated spectral patterns. Upper graphic: simulation EST; lower graphic: simulation MIE; from left to right, columns refer to: model function $S(n, f)$; averaged SPWVD $\widehat{S}(n, f)$; instantaneous frequencies and instantaneous powers. Estimated $\hat{F}_i(n)$ and $\hat{P}_i(n)$ are reported in black, values of the model in gray. Time-frequency resolution was {20 s, 7 mHz} and {5 s, 13 mHz} for EST and MIE simulations. $R = 1000$ realizations was used.

tions are given as the full-width at half maximum of $g(n)$ (Δ_t) and of the Fourier transform of $|h(k)|^2$ (Δ_f), respectively. Representative examples of TF estimates and estimation errors estimated as in (25) are given in Figs. 6 and 7. It is shown that in simulation EST the estimated parameters perfectly followed the transitory, with a mean estimation error $|\bar{E}_\phi| < 2.8\%$ in T_1 and $|\bar{E}_\phi| < 3.6\%$ in T_2. In simulation MIE, which is characterized by much stronger rates of variation, the indices estimated using the SPWVD followed the theoretical changes, even if with a higher percentual error.

6. Discussion

Applications of TF methods of analysis in biomedical signal processing have increased in the last years [2]. Nevertheless, the problem of how to generate signals with a given TF model function has been less studied. Only a small number of methods for the synthesis of non stationary processes whose TF representation was closest, in a least squares sense, to a given model function $S(n, f)$ were presented in the literature [22,23]. The importance of these studies lies in that models which allow to reproduce real-like signals with predetermined TF characteristics can be used to validate and compare different non-stationary signal processing techniques. Another application of the presented framework may concern the generation of controlled TV surrogate data to assess non linearity in non stationary time series or the significance of TV coherence function [10].

In this paper, two robust and flexible frameworks for generating non-stationary HRV signals following predetermined spectral patterns have been presented. Signals are modeled as time-varying stochastic processes characterized either by spectral components with controlled instantaneous powers and frequencies or by a given time-frequency model function, whose shape can be controlled by tuning several design parameters. Using these methods we were able to simulate stochastic signals whose spectral components changed both linearly and non-linearly during time, with different rates of variation, going from slow variations to sudden and very sharp transitions. We modeled HRV dynamics during exercise stress testing and experiments of music-induced emotions and we observed that using the smoothed pseudo Wigner–Ville dis-

tribution it was possible to reliably follow these dynamics. These frameworks can be used in all those studies which require the generation of simulated HRV signals. Moreover, even if in this study we only considered HRV dynamics, they could also be used to simulate any of those cardiovascular signals which present at least a LF or a HF component, e.g. arterial pressure variability, photoplethysmographic signal, pulse transit time, etc.

6.1. Models for non-stationary HRV generation

The presented methodologies are based on the identification of the polar configuration associated to a model function whose geometry can be controlled by the design parameters introduced in Section 2.4. The identification problem has a closed-form solution which is exact in the case of I-FS and approximate in the case of II-FP framework. Therefore, once that the design parameters have been chosen, the solution of (10), or (16), directly provides the parameters of the model used to generate signals characterized by the desired properties. Framework II-FP has the advantage of allowing to directly control the instantaneous power of LF and HF components, but, being based on a TV-AR model, it cannot provide much control on the shape of $S(n, f)$ which is constrained to be a sum of Lorentzian functions. The capability of tuning the shape of the model function $S(n, f)$ by properly choosing parameters $z_k(n)$, gives a great flexibility to the I-FS framework, which additionally was observed to generate signals whose spectral patterns followed more reliably the desired ones. The quantification of the intrinsic uncertainty of the simulated signals through the estimation of d_W and $e(n)$ allows one to evaluate the signals before using them to assess a method of analysis. It was shown that the uncertainty increases with the magnitude of the poles. Thus, one should give to the magnitude of the poles used as design parameter the lowest value which at the same time provides a $S(n,f)$ which complies with the specifications.

A correct positioning of zeros $z_k(n)$ increases the number of possible $S(n, f)$ which can be modeled. For example, as shown in Fig. 2, $z_k(n)$ can be used to control the degree of overlapping of LF and HF spectral peaks when their central frequencies are close. To separate the LF and HF spectral peaks without using $z_k(n)$, one could move $|p_{LF}|$ toward the unit circle which, in turn, has the undesirable
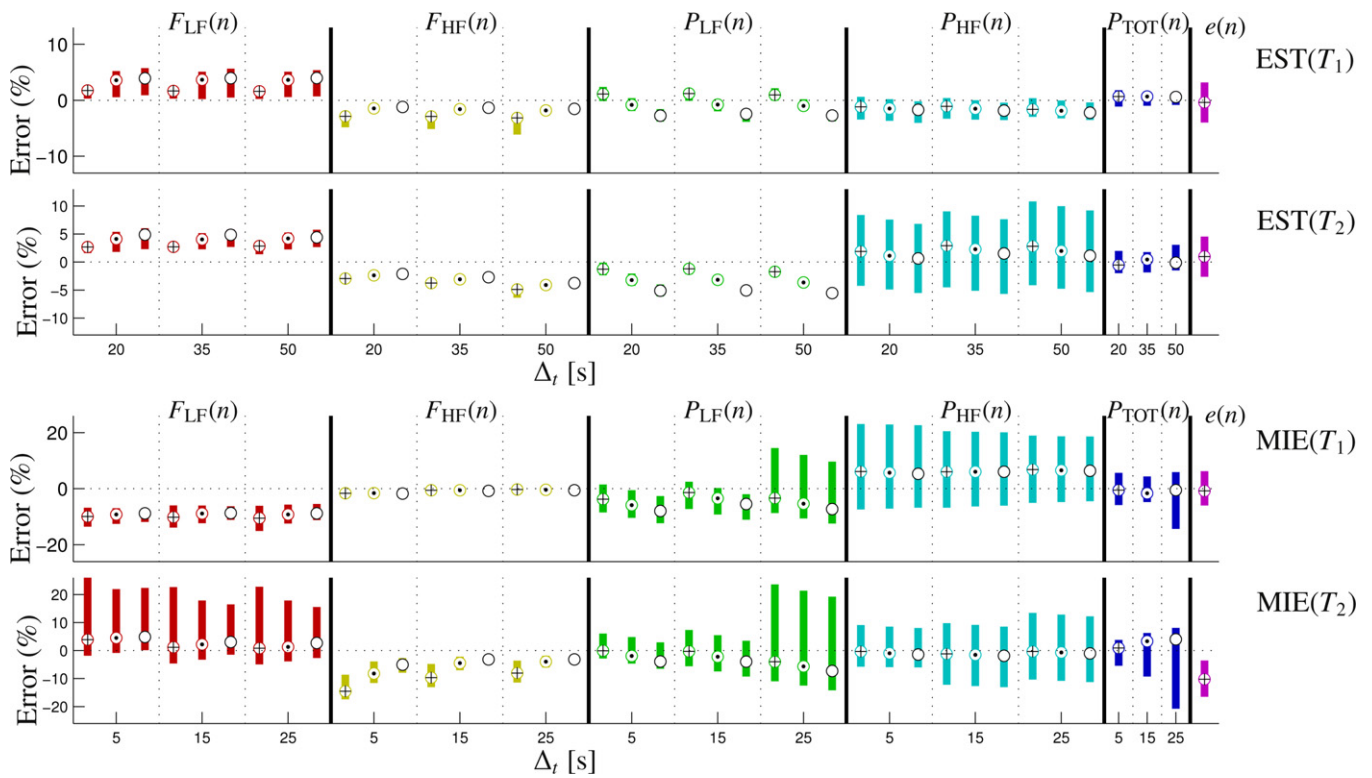
Fig. 7. Distribution of the estimation error E_ϕ for parameters $\phi = \{F_{LF}, F_{HF}, P_{LF}, P_{HF}, P_{TOT}\}$. In the last column the distribution of the uncertainty $e(n)$ is reported. Results obtained with a frequency resolution $\Delta_f = \{0, 7, 13\}$ mHz are reported with a cross, a point and a circle, respectively. Symbols represent the median values and the box extremities represent the 25th and the 75th percentiles.

effect of increasing the uncertainty of the signals. Thus, the use of TV-ARMA models instead of the simpler TV-AR models is crucial not only to improve the control of $S(n, f)$ but also to reduce the intrinsic uncertainty of the simulated signals. In some configurations, additional $z_k(n)$ should be used to compensate for the introduction of undesirable components in $S(n, f)$. In the applications presented in this paper, $z_k(n)$ were placed on the unit circle. In those applications where this constraint is too restrictive, $S(n, f)$ could be forced to a non-zero value by placing the $z_k(n)$ inside the unit circle, as shown in Fig. 2. The model sampling rate F_s is another important parameter. It should be high enough to ensure a good time resolution but not too high, in order to spend the degrees of freedom of the model to describe relevant signal components and not modeling noise presents in high frequency band. The presented frameworks have been shown to be robust: as shown in Fig. 5 it was possible to find a pole-zero configuration for any kind of possible combination of HRV spectral indices.

6.2. The SPWVD for HRV quantification

One of the more relevant applications of signal synthesis methods is the validation of signal processing techniques, whose limitations should be known by users, in order to make a correct interpretation of the results. Among all the TF representations, the WVD is characterized by the best TF resolution, but its applicability is limited by the presence of interference terms. These terms are reduced by low-pass filtering the WVD by means of TF kernels. The SPWVD, which makes use of separable kernels, is one of the most appealing solution due to the possibility of an independent filtering in time and frequency. For a comprehensive description of TFR representations see [19]. As reported in Fig. 6–7, during both simulations EST and MIE, the SPWVD estimated the dynamic of the simulated signals with a median error which, in the worst case,

did not exceed the 10%. Results should be compared to the intrinsic uncertainty of the simulated signals, whose distribution is reported in the last column of Fig. 7. The estimation error $E_\phi(n)$ increased by increasing the rate of variation of the spectral components. For simulation EST, the estimation error was always very low, both for epochs T_1 and T_2. The time-course of $F_{LF}(n)$, $F_{HF}(n)$ and $P_{LF}(n)$ was estimated with an estimation error whose median and interquartile range were bounded between 0.78% and 5.52% and between 0.29% and 5.16%, respectively. During T_2, the interquartile range of the estimation error of $\hat{P}_{HF}(n)$ was higher, but still comparable with that of $e(n)$, which measures the intrinsic uncertainty. The temporal evolution of the total power was estimated with an error whose median and interquartile range were bounded between 0.11% and 0.65% and between 2.11% and 4.55%, respectevely. For simulation MIE, the estimation error was higher, especially during T_2. Nevertheless, in Fig. 6, it is shown that $\hat{P}_{LF}(n)$ and $\hat{P}_{HF}(n)$ correctly followed the temporal evolution of $P_{LF}(n)$ and $P_{HF}(n)$ even during T_2. In this simulation, the estimation of $P_{LF}(n)$ worsened by increasing the degree of the time-smoothing. To correctly track the changes of the HRV spectral indices, one should always pay attention to the TF resolution given by the kernels. Concerning the effect of the TF filtering, it is shown that the estimation error of $P_{TOT}(n)$ only depended on the filtering in time, and that for a given time resolution, $E_\phi(n)$ decreased by increasing the degree of the frequency filtering. This was particularly evident for the estimation of HF instantaneous power and frequency, where misestimations due to residual interference terms are more frequent. The use of a time-varying respiration-dependent boundaries [21] was very effective to improve the estimation of the HF component, which otherwise would have required a much higher degree of filtering.

In this paper we used a rather basic TF analysis, which involves a TF filtering of the WVD by means of time-invariant kernels which were arbitrary chosen, and an estimation of spectral indices by inte-

grating $\hat{S}(n,f)$ in B_{LF} and $B_{HF}(n)$. More sophisticated techniques have been presented in the literature to improve the spectral characterization of non-stationary signals. An interesting possibility is to make the TF filtering of the WVD time-varying or signal-dependent [24]. Another possibility is to perform a parametric decomposition of the generalized autocorrelation function [3]. A method, which combines parametric decomposition of the autocorrelation function with a dynamic adjustment of the TF filtering which depends to the rate of variation of the spectral components of the signal, has been recently proposed [6]. All these methodologies were assessed by means of deterministic signals embedded in noise. The frameworks presented in this paper could be used to further analyze their performance.

Acknowledgements

References

[1] Heart rate variability: standards of measurement, physiological interpretation and clinical use. Task Force of the European Society of Cardiology and the North American Society of Pacing and Electrophysiology, Circulation 93 (5) (1996) 1043–1065.

[2] L.T. Mainardi, On the quantification of heart rate variability spectral parameters using time-frequency and time-varying methods, Philos. Trans. Ser. A: Math. Phys. Eng. Sci. 367 (1887) (2009) 255–275.

[3] L.T. Mainardi, N. Montano, S. Cerutti, Automatic decomposition of Wigner distribution and its application to heart rate variability, Meth. Infor. Med. 43 (1) (2004) 17–21.

[4] H.L. Chan, H.H. Huang, J.L. Lin, Time-frequency analysis of heart rate variability during transient segments, Ann. Biomed. Eng. 29 (11) (2001) 983–996.

[5] L. Keselbrener, S. Akselrod, Selective discrete Fourier transform algorithm for time-frequency analysis: method and application on simulated and cardiovascular signals, IEEE Trans. Biomed. Eng. 43 (8) (1996) 789–802.

[6] R. Bailón, L. Mainardi, M. Orini, L. Sörnmo, P. Laguna, Analysis of heart rate variability during exercise stress testing using respiratory information, Biomed. Signal Process. Control 5 (4) (2010) 299–310.

[7] L. Glass, Synchronization and rhythmic processes in physiology, Nature 410 (6825) (2001) 277–284.

[8] O. Meste, B. Khaddoumi, G. Blain, S. Bermon, Time-varying analysis methods and models for the respiratory and cardiac system coupling in graded exercise, IEEE Trans. Biomed. Eng. 52 (11) (2005) 1921–1930.

[9] A.M. Bianchi, L.T. Mainardi, E. Petrucci, M.G. Signorini, M. Mainardi, S. Cerutti, Time-variant power spectrum analysis for the detection of transient episodes in HRV signal, IEEE Trans. Biomed. Eng. 40 (2) (1993) 136–144.

[10] H. Zhao, W.A. Cupples, K.H. Ju, K.H. Chon, Time-varying causal coherence function and its application to renal blood pressure and blood flow data, IEEE Trans. Biomed. Eng. 54 (12) (2007) 2142–2150.

[11] R. Bailón, J. Mateo, S. Olmos, P. Serrano, J. Garcia, A. del Rio, I.J. Ferreira, P. Laguna, Coronary artery disease diagnosis based on exercise electrocardiogram indexes from repolarisation, depolarisation and heart rate variability, Med. Biol. Eng. Comput. 41 (5) (2003) 561–571.

[12] M. Virtanen, M. Kähönen, T. Nieminen, P. Karjalainen, M. Tarvainen, T. Lehtimäki, R. Lehtinen, K. Nikus, T. Kööbi, M. Niemi, K. Niemelä, V. Turjanmaa, J. Malmivuo, J. Viik, Heart rate variability derived from exercise ECG in the detection of coronary artery disease, Physiol. Meas. 28 (10) (2007) 1189–1200.

[13] R. Bailón, P. Serrano, P. Laguna, Influence of time-varying mean heart rate in coronary artery disease diagnostic performance of heart rate variability indices from exercise stress testing, J. Electrocardiol., doi:10.1016/j.jelectrocard.2011.02.001.

[14] L. Bernardi, C. Porta, G. Casucci, R. Balsamo, N.F. Bernardi, R. Fogari, P. Sleight, Dynamic interactions between musical, cardiovascular, and cerebral rhythms in humans, Circulation 119 (25) (2009) 3171–3180.

[15] M. Orini, R. Bailón, R. Enk, S. Koelsch, L.T. Mainardi, P. Laguna, A method for continuously assessing the autonomic response to music-induced emotions through HRV analysis, Med. Biol. Eng. Comput. 48 (5) (2010) 423–433.

[16] S.J. Johnsen, N. Andersen, On power estimation in maximum entropy spectral analysis, Geophysics 43 (4) (1978) 681–690.

[17] G. Baselli, A. Porta, O. Rimoldi, M. Pagani, S. Cerutti, Spectral decomposition in multichannel recordings based on multivariate parametric identification, IEEE Trans. Biomed. Eng. 44 (11) (1997) 1092–1101.

[18] W. Martin, P. Flandrin, Wigner–Ville spectral analysis of nonstationary processes, IEEE Trans. Acoust. Speech Signal Process. 33 (6) (1985) 1461–1470.

[19] P. Flandrin, Time-frequency/Time-scale Analysis, Academic Press, NY, 1999.

[20] G. Blain, O. Meste, S. Bermon, Influences of breathing patterns on respiratory sinus arrhythmia in humans during exercise, Am. J. Physiol. Heart Circ. Physiol. 288 (2) (2005) H887–H895.

[21] R. Bailón, P. Laguna, L.T. Mainardi, L. Sornmo, Analysis of heart rate variability using time-varying frequency bands based on respiratory frequency, in: Proc. 29th Annual International Conference of the IEEE Engineering in Medicine and Biology Society EMBS 2007, 2007, pp. 6674–6677.

[22] G. Boudreaux-Bartels, T. Parks, Time-varying filtering and signal estimation using Wigner distribution synthesis techniques, IEEE Trans. Acoust. Speech Signal Process. 34 (3) (1986) 442–451.

[23] F. Hlawatsch, W. Kozek, Second-order time-frequency synthesis of nonstationary random processes, IEEE Trans. Inform. Theory 41 (1) (1995) 255–267.

[24] R.G. Baraniuk, D.L. Jones, A signal-dependent time-frequency representation: optimal kernel design, IEEE Trans. Signal Process. 41 (4) (1993) 1589–1602.